Materials Science and Engineering A 527 (2010) 6283–6288

Contents lists available at ScienceDirect

Materials Science and Engineering A

journal homepage: www.elsevier.com/locate/msea

Comparative property study on extruded Mg–HAP and ZM61–HAP composites

Asit Kumar Khanra[a,*], Hwa Chul Jung[b], Kug Sun Hong[b], Kwang Seon Shin[b,*]

[a] Department of Metallurgical and Materials Engineering, National Institute Technology, Hanamakonda, Warangal- 506 004, India
[b] Magnesium Technology Innovation Center, Research Institute of Advanced Materials (RIAM), School of Materials Science and Engineering, Seoul National University, 599 Gwanak-ro, Gwanak-gu, Seoul 151-744, Republic of Korea

ARTICLE INFO

Article history:
Received 12 December 2009
Received in revised form 8 June 2010
Accepted 10 June 2010

Keywords:
Mg
HAP
Extrusion
Hardness
SEM
Compressive strength

ABSTRACT

Present investigation explored the development of Mg–HAP (magnesium-hydroxyapatite) and ZM61–HAP composites by melting and extrusion route. The ZM61 matrix consisted of 93 wt% Mg, 6 wt% Zn and 1 wt% Mn. The different amounts of chemically synthesized HAP powder (0, 5, 10, and 15 wt%) were added to Mg melts and mechanical stir was used for the dispersion of HAP particles in the matrix. The as-cast billets were subjected to homogenization at 450 °C and finally extruded at 320 °C. The presence of HAP particles during extrusion resulted in decrease of grain size of the composites. The ZM61–HAP composites showed finer grain and higher hardness than Mg–HAP composites. The tensile and compressive properties of ZM61–HAP were found to be higher than Mg–HAP composites.

1. Introduction

Magnesium is the most highlighted and interesting implants for this century due to its biodegradability in nature. Many biomaterials have been developed over a few decades for the replacement of bone tissue. The metallic materials are found to be suitable biomaterials compared to the ceramic/polymeric counterparts due to combination of load bearing capacity and suitable mechanical and metallurgical properties. Generally, three types of metallic materials such as austenitic stainless steel (SS), Co–Cr alloys and pure Ti and its alloys are being used for surgical implants [1,2]. *In vivo* application of implant materials like plates, screw and pins require removal after healing of tissue by second surgical operation, which is unhealthful to the patient with extra surgical cost. It may be noted that the degradation of these metallic materials leads to toxic product, which results in loss of biocompatibility or loss of bone tissue. The property mismatch of natural bone and implant materials may leads to generation of stress and instability of implants [1].

The physical and mechanical properties of natural bone are found to differ with that of conventional metallic implants but quite similar to pure magnesium. Magnesium is the fourth abundant cation in human body (~1 mol/adult) and mainly found in bone tissue and it stabilizes the DNA and RNA structures [1]. Initially Mg based materials are first introduced as implant material due to its excellent biocompatibility but high corrosion rate of Mg alloys leads to application of more corrosion resistance materials such as stainless steel, Ti, etc. It is also found that different Mg based alloys such as AZ91, AZ31, WE43 and LAE442 show localized corrosion during *in vitro* and *in vivo* tests [3–6]. It is reported that many researchers are also trying to use biodegradable Mg as coronary stent materials and its performance is quite optimistic as compared to the permanent stents materials such as SS, Ta, Ti, NiTi, Co–Cr, Pt–Ir, etc. [7–9].

Much attention has already been paid on calcium based biomaterials such as HAP ($Ca_{10}(PO_4)_6(OH)_2$), and β-TCP ($Ca_3(PO_4)_2$) for the bone graft substitute due to their excellent biocompatibility, bioactivity and osteoconductive properties [10–15]. The calcium phosphate group is the largest inorganic materials of bone tissue and extensively used for orthopedic and dental application [16]. The HAP has unique feature of biocompatibility than other phosphate groups. The HAP particles show very low solubility as compared to β-TCP in our body fluid [10].

However, poor load bearing capability of HAP results in limited applications. The combination of metallic materials and HAP would be a promising approach to fabricate a metal matrix composites (MMC) as biomaterials. Different physical and mechanical properties of implants are presented in Table 1 [1]. The important properties such as compressive yield strength and fracture toughness of HAP are better than those of natural bone. The addition of small amount of HAP as a reinforcement to the biocompatible Mg matrix would be better option to achieve optimum properties.

* Corresponding authors.
E-mail addresses: asit@nitw.ac.in, asit_iitkgp@yahoo.com (A.K. Khanra), ksshin@snu.ac.kr (K.S. Shin).

0921-5093/$ – see front matter © 2010 Elsevier B.V. All rights reserved.
doi:10.1016/j.msea.2010.06.031

Table 1
Different physical and mechanical properties of implants in comparison to natural bone.

Properties	Natural bone	Magnesium	Synthetic HAP
Density (g/cc)	1.8–2.1	1.74–2.0	3.1
Elastic modulus (GPa)	3–20	41–45	73–117
Compressive yield strength (MPa)	130–180	65–100	600
Fracture toughness (MPa $m^{1/2}$)	3–6	15–40	0.7

Several metal matrix composites such as Ti–HAP, Ti–6Al–4V–HAP, AZ91–HAP, etc. have been developed to obtain the required properties [17–19]. The Mg based matrix would be better than Ti matrix from a biocompatibility point of view. The AZ91 alloy contains 9 wt.% Al, which has detrimental effect on human beings especially when it is used as biodegradable implants for bone replacement. Manufacturing of biomaterials by powder metallurgy route leads to extra production cost as compared to other technique. It is essential to fabricate biocompatible composite materials by using low costly process. Till now, there is no report on development of ZM61–HAP composite, wherein the addition of Zn, and Mn to Mg matrix may enhance mechanical properties as compared to pure Mg matrix.

Present study attempts to produce biocompatible Mg–HAP and ZM61–HAP composites by using chemically synthesized HAP particles. The microstructure and mechanical properties of the composites are evaluated.

2. Experimental procedures

In the present investigation, laboratory reagent grade $Ca(OH)_2$ powders (99% purity, High Purity Co., Japan) and H_3PO_4 (85% purity, Junsei Chemicals Co., Korea) powders were used for chemical synthesis. Calculated amount of $Ca(OH)_2$ and H_3PO_4 powders were dissolved in 450 ml of distilled water separately to maintain stoichiometry of HAP (Ca/P: 1.67). Then both solutions were mixed in a beaker and ultrasonically stirred for 3 h. The white slurry was filtered and dried at 90 °C. The dried cake was calcined at 1100 °C for 4 h and finally the calcined product was crushed. The detailed description of chemical synthesis of HAP powders is explained elsewhere [20]. The HAP powders were characterized by X-ray diffraction (XRD) (M18XHF-22-SRA, Mac Science Co., Japan) and scanning electron microscope (SEM) (JEOL, JSM 630).

Pure Mg (99.9%) ingot was melted in a stainless steel crucible under the protection of gas mixture containing SF_6 and CO_2. The different amounts of HAP powders (0, 5, 10 and 15 wt%) were added slowly to the molten Mg at 700 °C and a special stirring system was used to achieve better distribution of HAP particles in the Mg matrix. In case of ZM61-HAP composite, calculated amounts of Zn and Mn were added to Mg melt and then appropriate amounts of HAP powder were added to the ZM61 matrix. A special cooling system was employed during solidification in order to obtain better mechanical properties of the composites. After solidification, the ingots were subjected to homogenizing treatment at 400 °C for 12 h. The homogenized ingots were machined, which were used as raw materials for extrusion (Yoo Chang, Korea). The extrusion of billets was performed at 320 °C.

Different physical and mechanical properties of the composites were evaluated by using the extruded samples. The density of different samples was measured by Archimedes principle at 25 °C using distilled water as medium with an error of ±0.01%. An average of 5 readings was taken for each reported density. The phase analysis of samples was performed by XRD, whereas, microstructure of the composites was investigated by optical microscope (OM). The samples were prepared by polishing on SiC papers and final polishing with diamond paste. The 5% nital solution was used as an etchant for composites, whereas a mixture of acetic acid (10 ml), picric acid (4.2 g), distilled water (10 ml) and ethanol (70 ml of 95% purity) was used for the etching of Mg–0 HAP (pure Mg) and ZM61–0 HAP (without HAP).

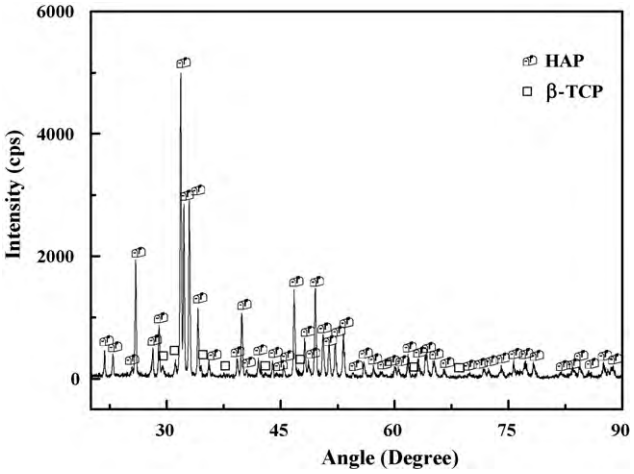

Fig. 1. XRD pattern of HAP powder.

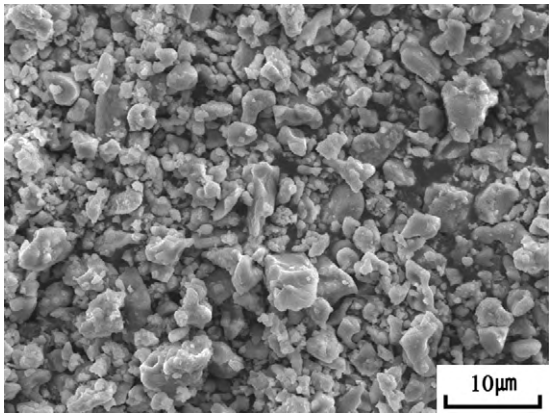

Fig. 2. SEM image of HAP powder.

The average grain size of the composite was measured by the line intercept method and a minimum of 400 grains were counted. The Vickers hardness of the sample was measured by a Wolpert hardness tester. The reported hardness values of the composites were the average of 15 readings. The cylindrical tensile and compressive specimens were machined along the extrusion direction of the rod, and tests were carried out at room temperature on an Instron testing machine at an initial strain rate of $2 \times 10^{-4}\,s^{-1}$. The sample sizes were taken according to the ASTM standard of E8 for tensile test and E9 for compressive test. The tensile sample had gauge length and diameter of 30.0 ± 0.1 mm and 6.0 ± 0.1 mm, respectively. Both side of the sample had treaded grip of 19.0 ± 2.5 mm and total length was 101.6 ± 0.1 mm. The compression test sample had diameter and length of 10 mm and 12 mm, respectively. The morphology of fracture surface of tensile tested sample was investigated by SEM.

3. Results and discussion

The XRD pattern of calcined powder is shown in Fig. 1. The powder consists of HAP (JCPDS file: 74-0566) as a major phase with β-TCP (JCPDS file: 25-0378) (tricalcium phosphate) as a minor phase. The volume fraction of HAP and β-TCP are calculated from the XRD pattern and the amounts are found to

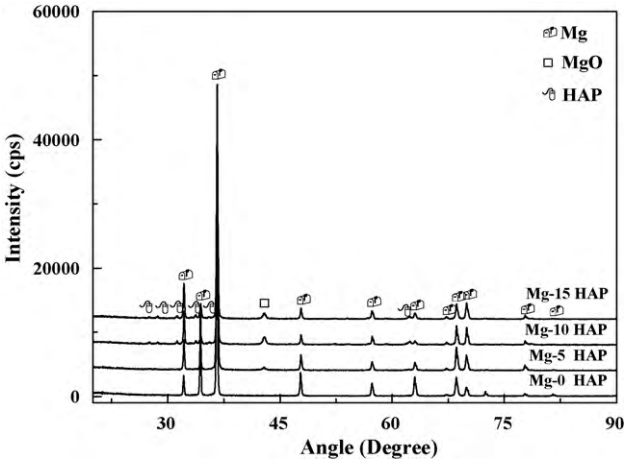

Fig. 3. XRD patterns of Mg–HAP composites.

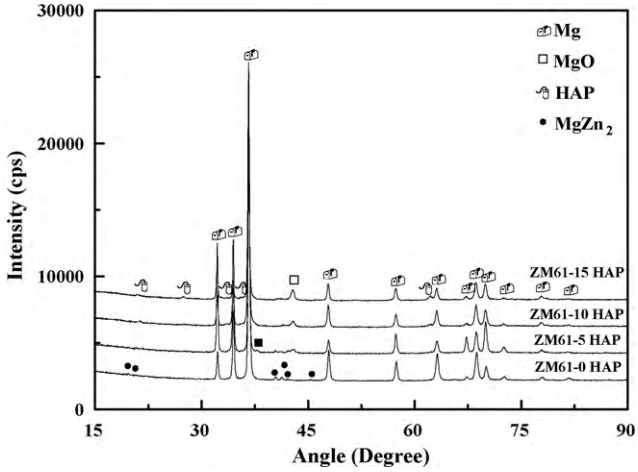

Fig. 4. XRD patterns of ZM61–HAP composites.

be ~94.46 and ~5.33 vol.% for HAP and β-TCP, respectively. The volume fractions of HAP and β-TCP phase were calculated on the basis of the area ratio of highest intensity peak of each phase. It has been reported that the dissolution rate of HAP in human body is low, whereas β-TCP has high dissolution rate [10]. The presence of biphasic apatite is useful to achieve the optimum restorability of the materials. The restorability of biphasic apatite is determined by the HAP/β-TCP ratio. Therefore, the presence of β-TCP as a minor phase in HAP powders is a bonus from the biocompatibility point of view. The SEM observation reveals the morphology of calcined powders (Fig. 2). The powder consists of agglomeration of fine particles (1–5 μm) and the shape of the particle is mainly nonspherical and angular types.

The theoretical density of the composites is measured to be 98–99%. The XRD patterns of different extruded composites are shown in Figs. 3 and 4, respectively. Fig. 3 shows presence of HAP and MgO (JCPDS file: 78-0430) as minor phase in case of Mg–HAP composites. Presence of β-TCP phase is not detected by XRD study, which could be due to its low crystallinity nature. The presence of MgO in Mg–HAP composites indicates there is some interaction between Mg and HAP during production. It has also been observed the presence of MgO in as-cast Mg–HAP composites. This indicates that during melting process, the Mg and HAP reacts to form MgO. The chances of reaction between adsorbed water in HAP and pure Mg is very small because MgO phase also forms by using preheated (200 °C) HAP powders. A similar type of trend is also observed in case of ZM61–HAP composites (Fig. 4). During melting, the Mg and Zn react to form a new $MgZn_2$ phase (JCPDS file no: 01-1211).

The optical micrographs of the composites shows decrease of grain size due to the addition of HAP (Fig. 5). The average grain size of Mg–0 HAP is found to be ~27 μm, whereas the grain size

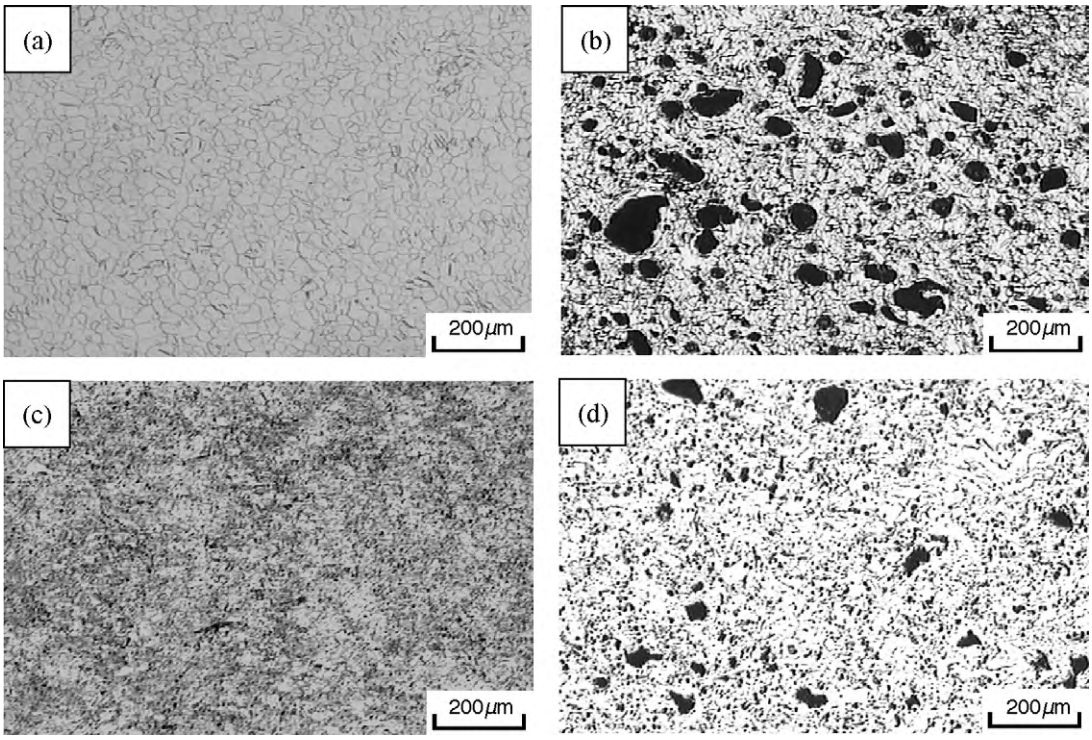

Fig. 5. Microstructure of composites: (a) Mg–0 HAP, (b) Mg–10 HAP, (c) ZM61–0 HAP, and (d) ZM61–5 HAP.

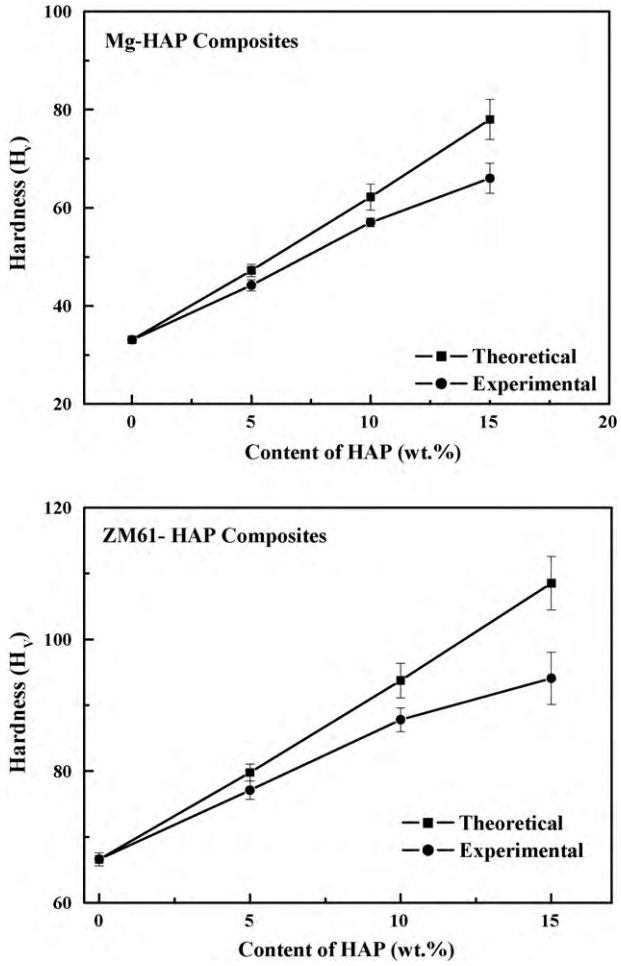

Fig. 6. Relationship between theoretical and experimental hardness of composites.

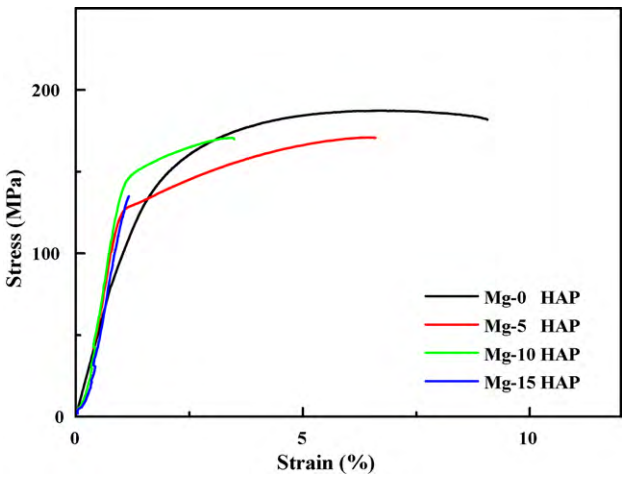

Fig. 7. Tensile stress–strain curves of Mg–HAP composites.

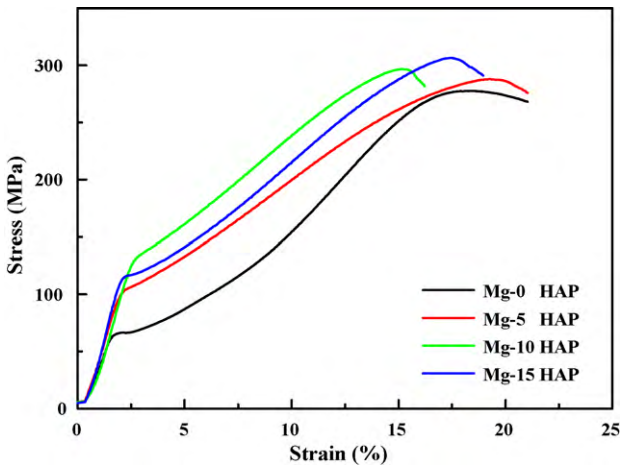

Fig. 8. Compressive stress–strain curves of Mg–HAP composites.

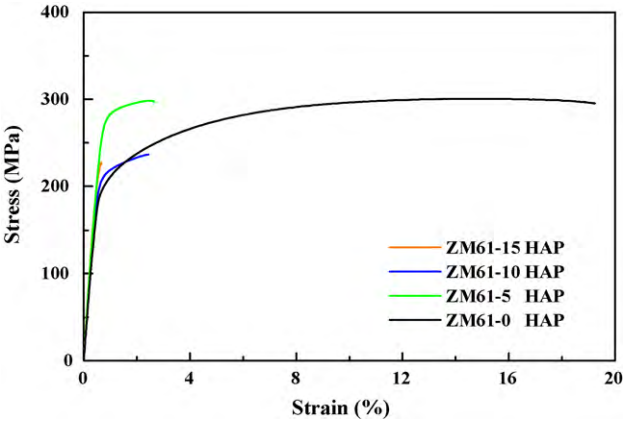

Fig. 9. Tensile stress–strain curves of ZM61–HAP composites.

decreases to ~15 μm in case of Mg–10 HAP. The presence of HAP particles in the Mg matrix during extrusion is responsible for the grain refinement. The detailed information on the effect of HAP on Mg matrix is reported by Khanra *et al.* [20]. The extrusion pressure is found to increase with the addition of HAP. Similar results could be expected in case of ZM61–HAP composites. The microstructure could not reveal exact information due to fine grain structure of the composites (Fig. 5c and d). Different hardness plots of the composites are shown in Fig. 6. The hardness values are calculated from the volume fraction and hardness of individual matrix (Mg, ZM61) and HAP. The hardness of 99% sintered HAP is used as a reference hardness value for HAP [16]. The nonuniform distribution of HAP in the matrixe results in lower experimental hardness than the theoretical value. Tensile and compressive stress–strain curves of the Mg–HAP composites are presented in Figs. 7 and 8, respectively. The tensile strength of the Mg–HAP composites is found to decrease with the addition of HAP. A maximum tensile strength of ~188 MPa is observed for Mg–0 HAP, whereas Mg–15 HAP shows minimum strength level of ~137 MPa. The addition of hard phase (HAP) may results in decrease of tensile strength of the composites. This indicates decrease of ductility with the HAP addition. It has also been observed that the elongation decreases with the HAP and this again attributed to increase of brittleness behaviour of the Mg–HAP composites. The compressive strength of the composite is found to increase with the addition of HAP (Fig. 8). This phenomenon indicates increase of hardness with HAP, which is close

Table 2
Results of tensile and compression tests for composites.

Sample	Tensile YS (MPa)	UTS (MPa)	Total strain (TS)	Compressive YS (MPa)	CS (MPa)
Mg–0 HAP	121.4	187.9	9.5	65.8	277.8
Mg–15 HAP	129.6	136.7	0.3	147.1	298.2
ZM61–0 HAP	195.7	301	14.7	141.2	355.6
ZM61–15 HAP	225.5	225.5	0.3	245.3	388.3

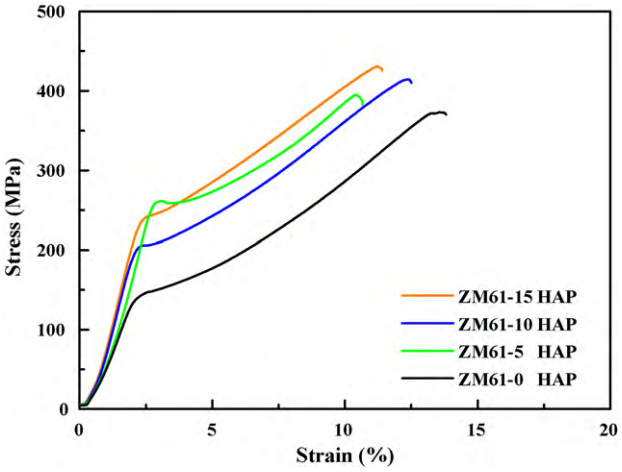

Fig. 10. Compressive stress–strain curves of ZM61–HAP composites.

agreement with the results of tensile strength behaviour of the composites. The Mg–15 HAP and Mg–0 HAP composite show compressive strength of ~305 and ~265 MPa, respectively. The results of tensile and compression tests for the composites are summarized in Table 2. The tensile yield strength decreases with the addition of HAP, whereas the compressive yield strength increases with HAP. The Mg–10 HAP composite shows higher yield strength than that of Mg–15 HAP, which could be due to in homogenious distribution of HAP in the matrix. The tensile and compressive curves of the ZM61–HAP composites are shown in Figs. 9 and 10, respectively. The ZM61–HAP composites show similar behaviour with that of the Mg–HAP composite. The tensile and compressive strength are found to be higher than those of the Mg–HAP composites (Table 2). The nonuniform distribution of HAP in ZM61 matrix results in nonsymmetrical trend in both plots in case of the ZM61–5 HAP composite. The higher viscosity of ZM61 matrix than Mg leads to more nonuniform distribution of HAP particles in matrix. This phenomenon is expected during the production of composites by melting route. The powder metallurgy route for fabrication of such composites is under progress to achieve better distribution of HAP particles.

The fractrography of the Mg–HAP composite after tensile tests are shown in Fig. 11. The Mg–0 HAP shows presence of dimples in the fractured surface. It can be considered that the superior ductile behavior of Mg–0 HAP is caused by dimple formation in the fracture surface. In case of the Mg–5 HAP, the elongation is decreased. Fig. 11 shows that pull out of HAP particles in the case of Mg–5 HAP and the decrease in yield strength can be explained by the formation of secondary cracks. The fractrographs of Mg–10 and 15 HAP in Fig. 11 show the flat plane, which indicate brittle fracture behavior of the Mg–HAP composites. Both samples show presence of agglomeration of HAP particles on the fracture surface. The agglomeration of HAP could cause brittle fracture in the composites with the addition of HAP (Fig. 7). Similar fracture behavior was observed in ZM61–HAP composites.

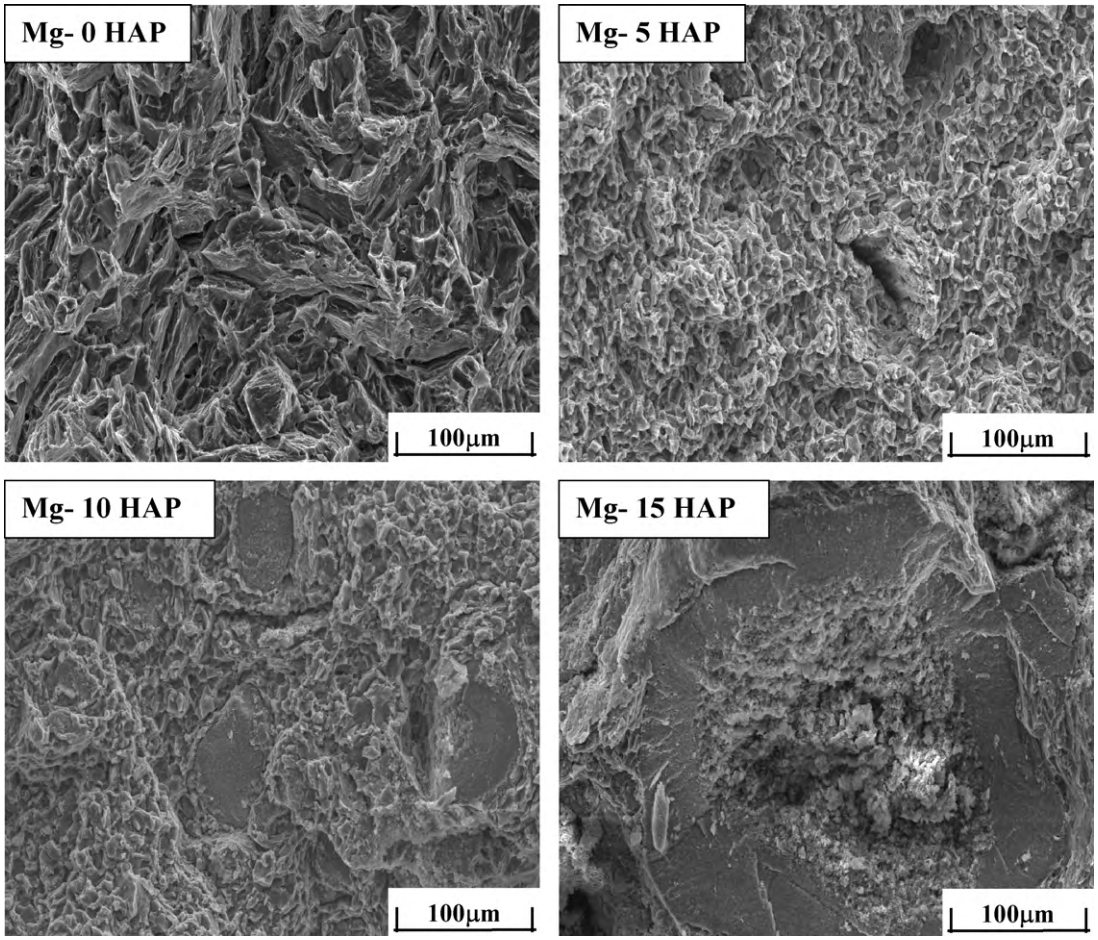

Fig. 11. Fractrographs of Mg–HAP composites.

4. Conclusions

The Mg based composites are produced by melting and extrusion route wherein chemically synthesized HAP powder is used as reinforcing agent. The microstructure study reveals the relation between the grain size of composites and the amount of HAP addition. The hardness, tensile and compressive strength of ZM61–HAP composites are found to be higher than Mg–HAP composites. The factography study reveals the ductile to brittle behaviour of composites.

Acknowledgement

This research work was financially supported by MTIC, RIAM, BK21 Materials Education and Research Division and the Fundamental R&D Program for Core Technology of Materials funded by the Ministry of Commerce, Industry and Energy, Republic of Korea through RIAM.

References

[1] M.P. Staiger, A.M. Pietak, J. Huadmai, G. Dias, Biomaterials 27 (2006) 1728–1734.
[2] S. Kannan, A. Balamurugan, S. Rajeswari, Mater. Lett. 57 (2003) 2382–2389.
[3] F. Witte, V. Kaese, H. Haferkamp, E. Switzer, A.M. Lindenberg, C.J. Wirth, H. Windhagen, Biomaterials 26 (2005) 3557–3563.
[4] F. Witte, J. Fischer, J. Nellesen, H.A. Crostack, V. Kaese, A.P.F. Beckmann, H. Windhagen, Biomaterials 27 (2006) 1013–1018.
[5] F. Witte, H. Ulrich, M. Rudert, E.J. Willbond, J. Biomed. Mater. Res. A 81 (2007) 748–756.
[6] F. Witte, H. Ulrich, C. Palm, E.J. Willbond, J. Biomed. Mater. Res. A 81 (2007) 757–765.
[7] G. Mani, M.D. Feldman, D. Patel, C.M. Agrawal, Biomaterials 28 (2007) 1689–1710.
[8] J. Ormiston, M. Webster, Lancet 369 (2007) 1839–1841.
[9] R. Erbel, C.D. Mario, J. Bartunek, J. Bonnier, B. Bruyne, F.R. Eberli, H. Aude, B. Heublein, M. Horrigan, C. Ilsley, D. Bose, J. Koolen, T.F. Luscher, N. Weissman, R. Wakaman, Lancet 369 (2007) 1869–1871.
[10] S.H. Kwon, Y.K. Jun, S.H. Hong, H.E. Kim, J. Eur. Ceram. Soc. 23 (2003) 1039–1045.
[11] H.S. Ryu, H.J. Youn, K.S. Hong, B.S. Chang, C.K. Lee, S.S. Chung, Biomaterials 23 (2002) 909–914.
[12] J. Chakraborty, M.K. Sinha, D. Basu, J. Am. Ceram. Soc. 90 (2007) 1258–1261.
[13] W.L. Suchanek, K. Byrappa, P. Shuk, R.E. Riman, V.F. Janas, K.S. Tenhuisen, Biomaterials 25 (2004) 4647–4655.
[14] W.L. Suchanek, K. Byrappa, P. Shuk, R.E. Riman, V.F. Janas, K.S. Tenhuisen, J. Solid State Chem. 177 (2004) 793–798.
[15] S. Kannan, J.M. Ventura, J.M.F. Ferreira, Ceram. Int. 20 (2007) 1397.
[16] S. Paramanik, A.K. Agarwal, K.N. Rai, A. Garg, Ceram. Int. 33 (2007) 419–426.
[17] C.Q. Ning, Y. Zhou, Biomaterials 23 (2002) 2909–2915.
[18] E.S. Thian, N.H. Loh, K.A. Khor, S.B. Tor, Biomaterials 23 (2002) 2927–2938.
[19] F. Witte, F. Feyerabend, P. Maier, J. Fischer, M. Stromer, C. Blawert, W. Dietzel, N. Hort, Biomaterials 28 (2007) 2163–2174.
[20] A.K. Khanra, H.C. Jung, S.H. Yu, K.S. Hong, K.S. Shin, Bull. Mater. Sci. 33 (2010) 43–47.